The Gemini Planet Imager Calibration Wavefront Sensor Instrument

J. Kent Wallace*, Rick S. Burruss, Randall D. Bartos, Thang Q. Trinh,
Laurent A. Pueyo, Santos F. Fregoso, John R. Angione, J. Chris Shelton
Jet Propulsion Laboratory, California Institute of Technology, 4800 Oak Grove Drive,
Pasadena, CA, USA 91109;

ABSTRACT

The Gemini Planet Imager is an extreme adaptive optics system that will employ an apodized-pupil coronagraph to make direct detections of faint companions of nearby stars to a contrast level of the 10^{-7} within a few lambda/D of the parent star. Such high contrasts from the ground require exquisite wavefront sensing and control both for the AO system as well as for the coronagraph. Un-sensed non-common path phase and amplitude errors after the wavefront sensor dichroic but before the coronagraph would lead to speckles which would ultimately limit the contrast. The calibration wavefront system for GPI will measure the complex wavefront at the system pupil before the apodizer and provide slow phase corrections to the AO system to mitigate errors that would cause a loss in contrast. The calibration wavefront sensor instrument for GPI has been built. We will describe the instrument and its performance.

Keywords: adaptive optics, coronagraph, wavefront sensing, planet detection

1. INTRODUCTION

The feasibility of direct detection of young, Jupiter-class, self-luminous exoplanets from the ground has been clearly demonstrated with the observations of the multiple system around HR8799[1,2]. These detections pose significant engineering challenges, for existing AO systems. However, a new generation of systems that are to come on line soon[3,4,5] are designed specifically for these challenging targets. These new AO systems must have a large closed-loop bandwidth to correct for atmospheric phase errors and provide high instantaneous Strehls. For imaging faint companions close to the parent star, suppression of diffraction is crucial. Sensing and control of the smallest residual phase errors (on order of 1 nm, rms) is required to prevent creation of image plane speckles. This sensing and control must be done on the time scales over which the phase errors evolve, which is on the order of thirty seconds to a couple of minutes. Therefore, in order to reach the highest contrast levels, sensing and control must occur during the science exposure which typically is on the order of thirty minutes to one hour.

The Gemini Planet Imager (GPI) instrument will use a calibration wavefront sensor to do just that. The calibration wavefront sensor will take part of the science light (~ 20%) and measure the phase and amplitude errors that scatters the starlight into the science path. In this paper we will describe the fundamental operation of the instrument, describe some of the unique engineering challenges, and discuss the instrument performance.

1.1 Overview of the operation of the GPI Calibration wavefront sensor

There are two fundamental wavefront measuring operations of the calibration wavefront sensor divided into the low order and high order phase modes. A schematic image of the calibration system is shown below in Figure 1. The system is composed of two uniquely different sensors: the low-order and high-order wavefront sensors. The low-order modes include those aberrations that make their way through the focal plane mask of the coronagraph. The high-order modes are those modes in the pupil plane that scatter light into the science beam path. Necessarily, the cal sensor must then sample part of this light in order to make a measurement. Fundamentally then, the focal plane mask is a spatial filter that defines the separation between low and high orders. Each wavefront sensor is described in more detail below.

*James.K.Wallace@jpl.nasa.gov; phone 1 818 393-7066; fax 1 818 393-3290; jpl.nasa.gov

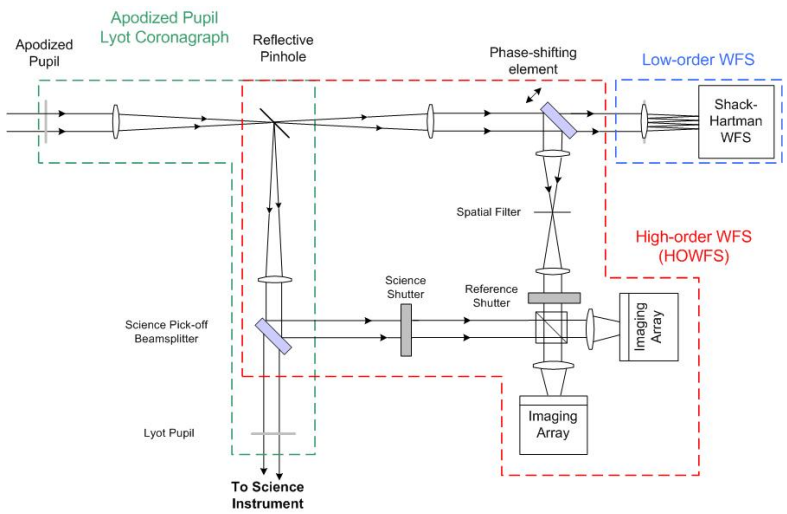

Figure 1. Schematic optical layout of the calibration wavefront sensor. Light from the telescope and adaptive optics system enters on the upper left. In the focal plane after the first lens is a reflective pinhole. Here, the vast majority of the bright starlight continues to the right while light from the faint, nearby companion is folded downward. Part of the bright starlight is sensed by the low-order wavefront sensor (LOWFS) shown in the blue dashed box. Light in the science arm is picked off by a beampslitter and recombined with some of the bright starlight. This forms an interferometer that is highlighted by the red dashed lines—the high order wavefront sensor (HOWFS).

1.2 Cal low-order wavefront sensor (LOWFS)

As illustrated in Fig. 1, light that passes through the hole in the focal plane mask is re-collimated and forms a real image of the pupil. Our optics then relay this pupil image to another image at the location of the lenslet array just before the infrared sensor. There are seven lenslets that span the pupil, the sub-sequent spots are then sampled by a quad cell of 2x2 pixels. The measured centroid motions at each of the quad cells are transformed into the corresponding phase map in the input pupil via a matrix multiply with our reconstructor. The reconstructor was generated using a detailed simulation that took into account the effects of the apodized pupil, the finite size of the focal plane mask, and the coarse sampling of the lenslet array.

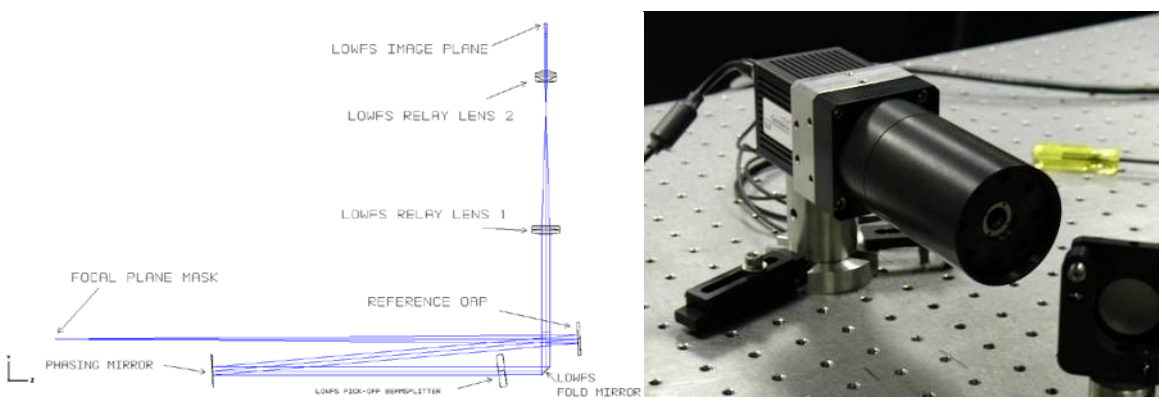

Figure 2. Details of the LOWFS are shown with above images. The optical layout of the system is shown with the layout of the left. It traces the light from the focal plane mask at the lower left of the image to an OAP, phasing mirror, pickoff beamsplitter and fold mirror. The LOWFS relay lenses are housed in the lens tube that attaches to the camera faceplate. The photograph on the left shows the LOWFS camera body as assembled for testing.

1.3 Cal High-order wavefront sensor (HOWFS)

Star light that is scattered around the mirror hole in the focal plane mask is re-collimated by optics that lead to the science instrument. In this beam path, a beamsplitter picks off a fraction of the light (~ 20%). This light is then recombined with a spatially filtered portion of the light rejected at the focal plane mask. The interfered light is then modulated by a phase shifting mirror in the reference arm.

At the recombination beamsplitter the electric fields for the science and reference are represented mathematically in equation 1. The magnitude and phase shift of the reference beam electric field are given by R and θ respectively.

$$E_{cal} = \frac{A}{2}(\varepsilon + i\varphi) + Re^{i\theta} \tag{1}$$

The intensity is then the squared modulus of the summed fields as shown in equation 2.

$$I_{cal} = \left|\frac{A}{2}(\varepsilon + i\varphi) + Re^{i\theta}\right|^2 \tag{2}$$

If we then take four phase steps with $\theta = 0, \pi/2, \pi, 3\pi/2$ and record the following pupil dependent intensities, we measure the following quantities.

$$\begin{aligned} I_1 &= \frac{A^2}{4}(\varepsilon^2 + \varphi^2) + R^2 + AR\varepsilon \\ I_2 &= \frac{A^2}{4}(\varepsilon^2 + \varphi^2) + R^2 + AR\varphi \\ I_3 &= \frac{A^2}{4}(\varepsilon^2 + \varphi^2) + R^2 - AR\varepsilon \\ I_4 &= \frac{A^2}{4}(\varepsilon^2 + \varphi^2) + R^2 - AR\varphi \end{aligned} \tag{3}$$

By taking appropriate differences and normalizing, it's possible to reconstruct the pupil-dependent phase and amplitude errors in pupil using the expression in equation 4.

$$\varphi = \frac{I_2 - I_4}{4I_0\left(\sqrt{REF}\sqrt{SCI}\right)}, \quad \varepsilon = \frac{I_1 - I_3}{4I_0\left(\sqrt{REF}\sqrt{SCI}\right)} \tag{4}$$

The performance of these two systems will be described in the next section.

2. CALIBRATION WAVEFRONT SENSOR PERFORMANCE

2.1 A description of the GPI Cal Instrument

The design of the GPI calibration instrument is dominated by the requirement that it be exceedingly rigid. This is for two reasons: 1) our high order system is a sensitive interferometer and must therefore be impervious to the pathlength fluctuations that can wash out the fringes during a measurement and 2) we are located at the Cassegrain focus of the telescope and thus presented with a variable orientation with respect to gravity. The calibration instrument is a box-like structure that is composed of a thick, light-weighted bottom and top plate. The internal bulkheads serve as opto/mechanical interfaces as well as stiffening elements for the whole structure. A diagram and image of the instrument is shown below in Fig. 3. All of our performance tests were done with this the final instrument configuration (but with the top lid on).

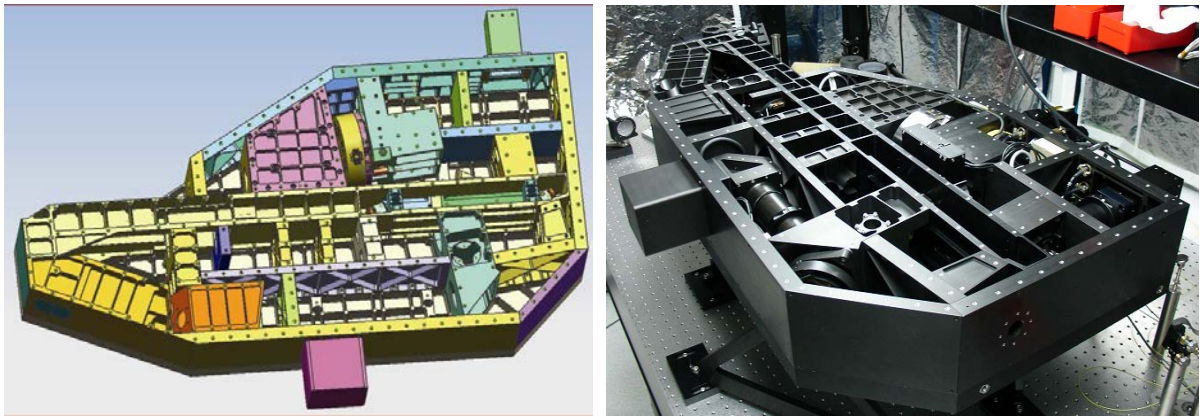

Figure 3. Solid drawing of the GPI Cal box, left, and an image of the final instrument hardware on the right. The square extensions on the sidewalls of the instrument are high and low order cameras.

2.2 LOWFS absolute accuracy

Validation of the LOWFS absolute accuracy consisted of first measuring a transparent phase aberration with a Zygo (we used a microscope slide), and then measuring the same slide with the LOWFS in the final Calibration instrument. The Cal instrument reconstructs the first 16 Zernike coefficients. The requirement for this absolute agreement is 5 nm, rms and we measured an agreement of 3.8 nm, rms.

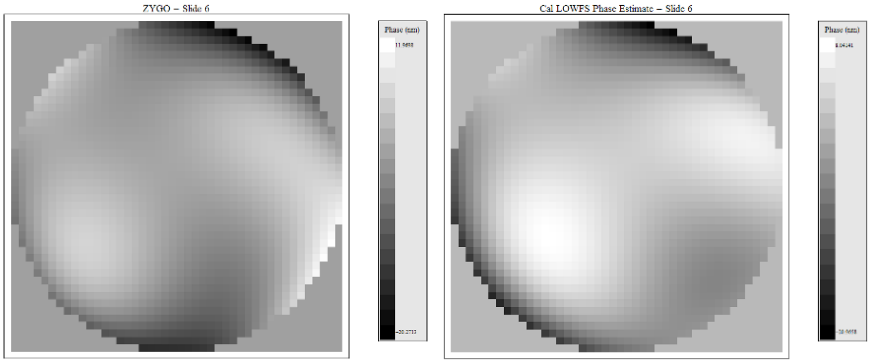

Figure 4. Absolute measurement accuracy of the Cal LOWFS. The image on the left is derived from the Zygo measurement of phase errors in a microscope slide. The image on the right is a measurement of the same slide with the LOWFS in our GPI Cal instrument. Absolute agreement to the 3.8 nm, rms level has been demonstrated.

2.3 LOWFS tip/tilt precision

A key requirement of our instrument is to act as the boresite for GPI. It's critical that it maintain good tip/tilt performance for different stellar magnitudes. In this test, we measured the tip/tilt noise in the LOWFS for different flux levels corresponding to the magnitudes shown below (Fig. 5). Our system can achieve pointing knowledge at the ~ two milliarcsec level in 20 secs at 8th magnitude.

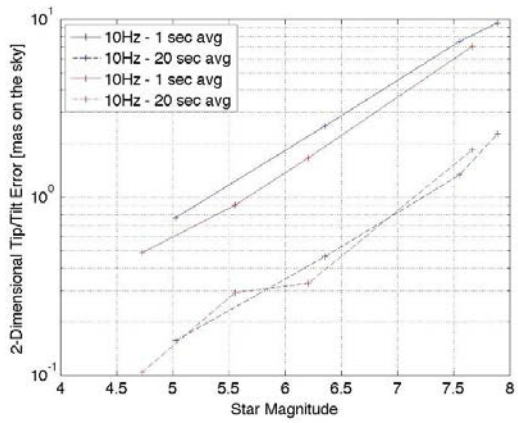

Figure 5. Precision of the LOWFS tip/tilt measurement for different stellar magnitudes. At 8th magnitude we can achieve point knowledge to 2 mas in 20 seconds.

2.4 HOWFS Absolute Accuracy

For the system to work well in closed loop, the HOWFS must also be able to make absolute measurements of the phase errors at the system pupil before the apodized pupil. Our characterization of absolute phase measurements for the HOWFS is identical to that used for the absolute measurements in the LOWFS. We measure the phase errors in a microscope slide first with a Zygo and then with the HOWFS in our Calibration wavefront sensor. The raw Zygo data is then used in a detailed, broadband simulation of the Calibration instrument. We get agreement from these two measurements at the ~4.5 nm, rms level. This is an absolute, open-loop measurement. When integrated with the rest of GPI we expect better performance in closed-loop.

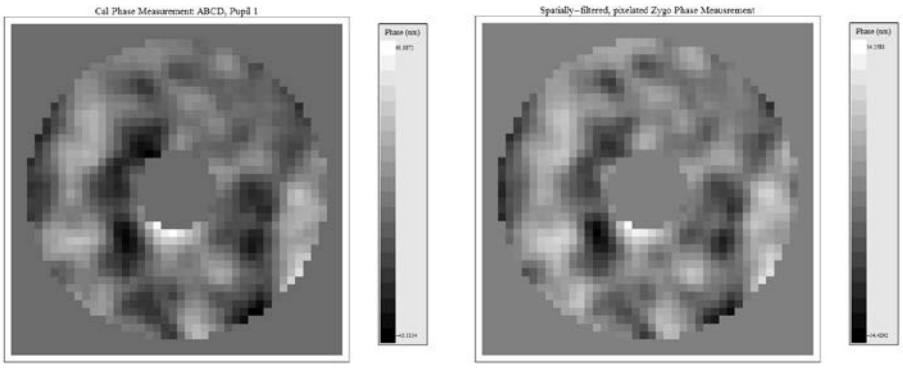

Figure 6. Absolute accuracy of the HOWFS instrument. The processed Zygo data of the microscope slide phase errors is shown on the left while the HOWFS measurement of the same microscope slide is shown on the right. Absolute agreement of these open loop errors is on the order of 4.5 nm, rms.

2.5 HOWFS Precision

For fainter stars the performance of the cal system is degraded. We validated the performance degradation in the lab by looking at the rms error in the reconstructed phase for different light levels. These measurements agree with our two requirements of 1 nm, rms in 1 minute at 5th magnitude and 12 nm, rms in 1 minute at 8th magnitude.

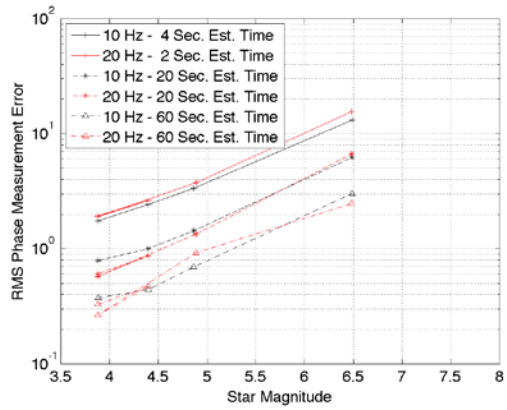

Figure 7. Degradation in the HOWFS performance as a function of stellar magnitude. These measurements were made with a single HOWFS pupil. These measurements agree with our two goals of 1 nm, rms in 1 minute at 5th magnitude and 12 nm, rms in 1 minute at 8th magnitude.

2.6 LOWFS Flexure

Given that our Calibration instrument defines the borsesite of the GPI instrument as a whole, it's important that it is stiff enough such that internal flexure isn't misinterpreted by the LOWFS as pointing error . We tested this effect in the lab by mounting our instrument on a flexure testing rig which allows us to rotate along one rotation axis a full 360 degrees. Our tip/tilt measurements over 90 degrees indicate that the cal instrument does indeed meet its stiffness requirements which was a tilt change of 1 mas per 10 degrees. The flexure testing rig is shown below in Fig. 8 and the results are shown in Fig. 9.

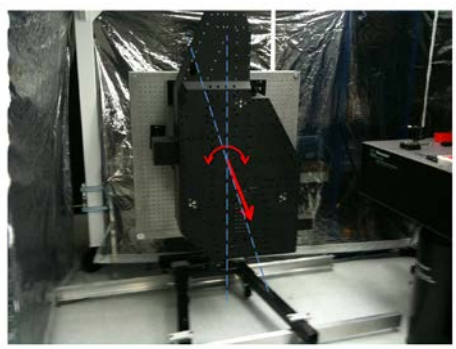

Figure 8. The GPI Calibration instrument loaded onto the flexure testing rig. The red arrow shows the rotation axis of the rig. The cal box was rotation a full +/- 45 degrees from the vertical dashed blue line..

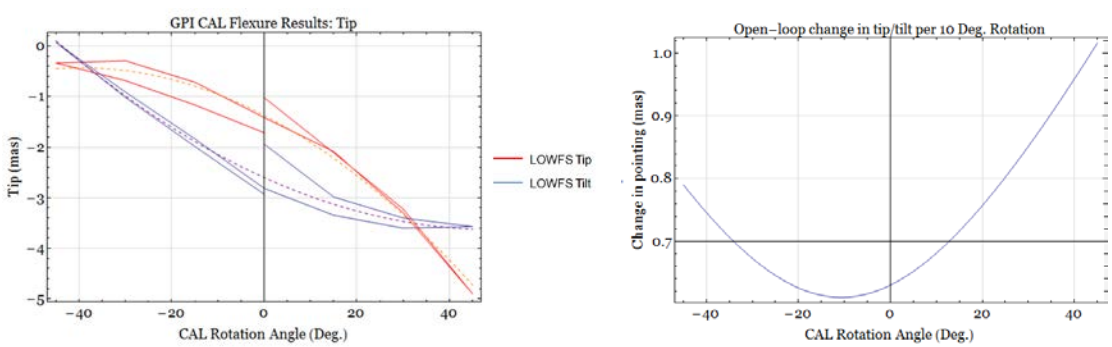

Figure 9. Results from the flexure tests. Absolute tip/tilt pointing is shown on the left and the pointing rate of change is shown on the right. The requirement of 1 mas per 10 degrees rotation is met over the range from -45 to 45 degrees.

3. SUMMARY AND CONCLUSION

Results of our validation of the performance of the GPI Calibration wavefront sensor instrument are in excellent agreement with the sub-system requirements. We are now in the early preparation for the next stage of the instrument---integration and test of our subsystem with the AO system and the science instrument.

4. ACKNOWLEDGEMENTS

This work was carried out by the Jet Propulsion Laboratory, California Institute of Technology, under contract with the National Aeronautics and Space Administration for the Gemini Observatory. The Gemini Observatory is operated by the Association of Universities for Research in Astronomy, Inc., under a cooperative agreement with the NSF on behalf of the Gemini partnership: the National Science Foundation (United States), the Particle Physics and Astronomy Research Council (United Kingdom), the National Research Council (Canada), CONICYT (Chile), the Australian Research Council (Australia), CNPq (Brazil), and CONICET (Argentina). This work has been supported in part by the National Science Foundation Science and Technology Center for Adaptive Optics, managed by the University of California at Santa Cruz under cooperative agreement No. AST-9876783.

REFERENCES

[1] Marois, C., et. Al., "Direct Imaging of Multiple Planets Orbiting the Star HR8799", *Science*, **322**, No. 5906, pp. 1348 – 1352 (2008).

[2] Serabyn, E., Mawet, D., Burruss, R., "An image of an exoplanet separated by two diffraction beamwidths from a star", *Nature*, **464**, 1018 (2010).

[3] Macintosh, B. A., Graham, J. R., Palmer, D. W., Doyon, R., Dunn, J., Gavel, D. T., Larkin, J., Oppenheimer, B., Saddlemyer, L., Sivaramakrishnan, A., Wallace, J. K., Bauman, B., Erickson, D. A., Marois, C., Poyneer, L. A., and Soummer, R., "The Gemini Planet Imager: from science to design to construction," *Proc. SPIE* **7015**, 31 (Jul 2008).

[4] Beuzit, Jean-Luc, Feldt, M., Dohlen, K., et.al., "SPHERE: a planet finder instrument for the VLT, SPIE Proc. 7014(2008).

[5] Bouchez, A., Dekany, R.,et.al., "The PALM-3000 High Order Adaptive Optics Upgrade for Palomar, Proc SPIE, (2008)